ACI MATERIALS JOURNAL TECHNICAL PAPER

Title No. 121-M20

Study on Effect of Curing Regimes on Ultra-High-Performance Concrete by Nuclear Magnetic Resonance Spectroscopy

by Hao Qian, Gaozhan Zhang, Jun Yang, Qingjun Ding, Chundong Geng, and Sudong Hua

As one of the key factors influencing the hydration process, as well as the microstructure formation and evolution of ultra-high-performance concrete (UHPC), the action mechanism of different curing regimes have been studied to some extent. However, the current knowledge of the underlying mechanisms that control the different effects of different curing regimes is limited. In this study, the composition of hydration products, micromorphology, and migration and evolution of aluminum-phase hydration products of UHPC under three combined curing regimes (standard curing, steam curing + standard curing, and autoclave curing + standard curing) were investigated in depth. Micromorphology observation shows that heat treatment promoted the formation of higher-stiffness hydration products (tobermorite and xonotlite) in UHPC, and the higher the polymerization degree, the higher the Si/Ca ratio of the hydration product. Meanwhile, ^{29}Si and ^{27}Al nuclear magnetic resonance (NMR) spectroscopy shows that specimens with higher strength had higher Al[4]/Si and a lower amount of ettringite and AFm at the early curing stage. The elevated curing temperature reduced the formation of ettringite and AFm and allowed more Al^{3+} to replace Si^{4+} into the structure and interlayer of the calcium-(alumino)silicate-hydrate (C-(A)-S-H) gel, which increased the mean chain length (MCL) and polymerization degree of the C-(A)-S-H gel. However, the polymerization effect of Al ions is limited, so the provision of the silicon source to improve the Si/Ca ratio of the system is important.

Keywords: calcium-(alumino)silicate-hydrate (C-(A)-S-H) gel; curing regime; nuclear magnetic resonance (NMR) spectroscopy; microstructure; ultra-high-performance concrete (UHPC).

INTRODUCTION

Ultra-high-performance concrete (UHPC) has been used in various construction applications because of its excellent permeability resistance, outstanding mechanical properties as well as durability, and superior ductility.[1-4] In bridge engineering, compared with ordinary concrete construction, UHPC could significantly reduce the volume and weight of piers, bridge girders, and other construction products and save a large amount of natural material.[5] However, due to the large amount of cementitious materials, low water-cement ratio, and compact design of UHPC, mineral admixtures with low reaction activity do not react immediately well in UHPC. Accordingly, the mechanical strength gain rate and hardening process of UHPC with standard curing are slow, which restricts the production rate construction activities and precast industries. Customized autoclaves are usually used for heat treatment in the factory production process. Although heat treatments such as autoclaved curing and steam curing have the disadvantage of limitation of specimen scale and the high cost of curing plant, heat treatment is essential to ensure the quality of products and improve production efficiency.[6-8] It was found that the heat treatment process in the production of precast UHPC products can greatly improve their early strength and volume stability.[9,10]

To provide guidance for the choice of appropriate curing regime and enhance the mechanical performance of UHPC, it is profound to study the influence of different curing regimes on the microstructure and hydration process of UHPC. The mechanisms of standard curing, steam curing, and autoclave curing, as the most commonly used curing regimes, have been studied in previous papers.[11-13] Shen et al.[14] investigated the effect of standard curing, steam curing, and autoclave curing on the mechanical properties and microstructure of UHPC. The results show that heat treatment could promote the generation of additional hydration products in UHPC. When the curing temperature reaches 90°C, the added silica fume/quartz powder could participate in the reaction with cementitious material in UHPC and generate fibrous or foiled tobermorite.[14,15] On continued increase of the curing temperature and pressure to 210°C and 2 MPa, respectively, the formed tobermorite ($Ca_{4+x}(H_{2-2x}Si_6O_{17})\cdot 5H_2O$)) is transformed into xonotlite ($Ca_6(Si_6O_{17})(OH)_2$).[11,16] However, the improved properties could not be obtained by simply prolonging the curing time and increasing the curing temperature. Higher curing temperature would harm the strength of UHPC at a later age.[17] Helmi et al.[18] found that heat curing alone (240°C) could accelerate the propagation of microcracks, which would make the 28-day compressive strength 5% lower than the 7-day compressive strength. Yazıcı et al.[19] also studied the effect of different curing conditions on UHPC, and the results show that curing temperature, pressure, and duration are all significant in the design of the curing regime. There was a specific curing time for each temperature and pressure. While the duration of heat treatment was short, the high-stiffness hydration product (such as tobermorite) was unstable. However, too long a curing time also had a negative influence due to the excessive crystallization. Moreover,

ACI Materials Journal, V. 121, No. 2, March 2024.

MS No. M-2022-418.R3, doi: 10.14359/51740372, received July 20, 2023, and reviewed under Institute publication policies.

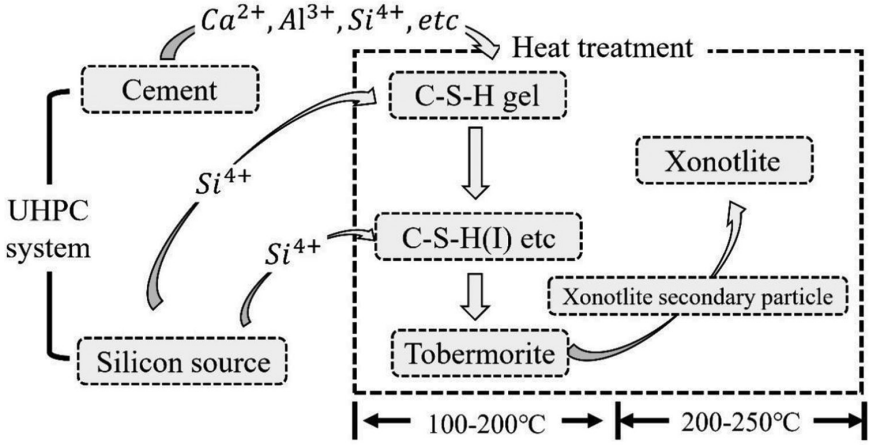

Fig. 1—Schematic diagram of hydration products' changes in UHPC under heat treatment.

the researches[19-21] found that an increase of curing pressure is helpful to improve the polymerization degree of hydration products and reduce curing time. Tobermorite could be detected at 6 hours of autoclaving at 1, 2, and 3 MPa and 10 hours of autoclaving at 0.5, 1, and 1.5 MPa. Although pressure treatment could result in an increase of specific gravity, the pressurization of entrapped air voids would promote the propagation of microcracks and reduce the strength. The Ca/Si ratio of calcium-silicate-hydrate (C-S-H) gel could reflect the polymerization degree of C-S-H gel in UHPC to some extent and evaluate the curing time of different curing regimes.[22,23] The Ca/Si ratio of C-S-H gel is usually between 0.8 and 2.5. When the Ca/Si ratio of the C-S-H structure reaches 0.8 to 1.0, C-S-H gel of this composition tends to convert to tobermorite first at temperatures between 100 and 200°C, and then to xonotlite at temperatures between 200 and 250°C.[14,19,24] To improve the polymerization degree of UHPC, the provision of an external silicon source is also important in the hydration process.[16] C_3S and C_2S could only convert to α-dicalcium silicate in the absence of silica fume/quartz powder (external SiO_2). Due to the higher porosity and smaller volume of α-dicalcium silicate, it is harmful to the strength of UHPC.

Generally, the evolution mechanism of hydration products in UHPC is shown in the schematic diagram in Fig. 1. Heat treatment promotes Al^{3+} to replace Si^{4+} in bridge sites of the silicate chains of C-S-H gel, which increases the mean chain length (MCL) and polymerization of silicate chains. The most predominant silicate chains in C-S-H gel transform from dimers to pentamers.[25,26] Before the formation of tobermorite, intermediate products such as C-S-H (I), C-S-H (II), and α-C_2SH are formed, which are harmful to the mechanical strength of UHPC due to their porous structures. With the increase in curing temperature and pressure, the pozzolanic reaction of the silicon source is intensified, and more Si^{4+} is released. The depolymerized Si^{4+} helps to convert the intermediate products into higher-stiffness hydration products (such as tobermorite and xonotlite).[27] The average stiffness of tobermorite and xonotlite are 77 and 106 GPa, respectively, which is much higher than that of C-S-H.[14,24] The higher stiffness of hydration products is beneficial to the improvement of mechanical properties of UHPC. Moreover, compared with intermediate hydration products, the tobermorite/xonotlite phase formed from the pozzolanic reaction has larger structural volume.[19] The pore-filling effect by tobermorite/xonotlite could reduce the porosity and drying shrinkage of UHPC and improve its compressive strength and resistance to chemical attack. As a result, although the role of curing pressure cannot be ignored, the enhancement effect of different curing regimes on the mechanical properties of UHPC is related to curing temperature.[14,28]

Many previous studies have shown the change of mechanical performance, microstructure, and hydration process of UHPC under different curing regimes. The reasons for the improvement of the mechanical properties of UHPC have been investigated from the perspective of microstructure. However, the current knowledge of the underlying mechanisms of long-term microstructural change with combined curing regimes is still limited. Presently, there are many researches on the difference between standard curing, steam curing, and water curing. There is little deep analysis of the composition of hydration products, C-S-H gel microstructure, and migration and evolution of aluminum-phase hydration products of cement/silica fume-quartz powder system UHPC under three curing regimes (standard curing at 20°C, steam curing at 90°C, and pressure steam curing at 210°C and 2 MPa). Therefore, it is necessary to pay attention to the study of the microstructural change behind different combined curing regimes. In this study, three types of typical combined curing regimes (standard curing, steam curing + standard curing, and autoclave curing + standard curing) were performed on UHPC specimens. The mechanical properties, microstructure, and the difference in improvement of three combined curing regimes were investigated. The microstructure development as well as migration and evolution of aluminum-phase hydration products of UHPC with different curing regimes is the research focus of this paper. The mechanical properties were characterized by testing the compressive strength of samples of different ages. Meanwhile, X-ray diffraction (XRD) and scanning electron microscopy (SEM) were used to investigate the hydration product and microstructure of specimen. The migration and evolution of Si and Al ions in UHPC were determined by ^{29}Si nuclear magnetic resonance (NMR) and

Table 1—Mixture proportions of cement, silica fume, and quartz powder

Constituent, wt%	SiO_2	Al_2O_3	Fe_2O_3	CaO	MgO	SO_3	K_2O	Na_2O	LOI
Cement	20.87	4.87	3.59	64.47	2.13	2.52	0.65	0.11	0.79
Silica fume	96.34	0.61	0.16	0.54	0.25	0.13	0.21	0.008	1.68
Quartz powder	98.75	0.73	0.11	0.06	—	—	0.16	—	0.19

Note: LOI is loss on ignition.

Table 2—Mixture proportions of UHPC, kg/m³

Cement	Silica fume	Quartz powder	River sand	Steel fiber	Water	HRWRA
880	265	325	1030	158	264	44.9

^{27}Al NMR spectroscopy, and the following main parameters were obtained: hydration degree of cement and silica fume/quartz powder, MCL, Al[4]/Si ratio.

RESEARCH SIGNIFICANCE

In this study, the composition of hydration products, micromorphology, and migration and evolution of aluminum-phase hydration products of UHPC under three combined curing regimes (standard curing, steam curing + standard curing, and autoclave curing + standard curing) were investigated in depth. By analyzing the underlying mechanism that controls the different effects of different curing regimes, it is expected to provide a reference for the selection of UHPC curing system. Moreover, it also provides a theoretical basis for the application of UHPC and further study of hydration reaction of UHPC.

MATERIALS AND EXPERIMENTAL METHODOLOGY

Materials

Raw materials—Portland cement (P.I 52.5) and mineral admixtures (silica fume and quartz powder) used in this study are all produced by domestic manufacturers. The specific surface area of silica fume and quartz powder were 19,500 and 445 m^2/kg, respectively. The chemical composition of portland cement, silica fume, and quartz powder are all shown in Table 1. Fine river sand with a fineness modulus of 1.87, derived from Yueyang Dongting Lake Yellow Sand, was used as aggregate in UHPC. Moreover, high-range water-reducing admixture (HRWRA) (water-reducing ratio of 30%, solid content of 20%), steel fiber (length = 13 mm, diameter = 0.18 mm, modulus of elasticity = 200 GPa) were also used. Tap water was used for mortar preparation and deionized water was used for UHPC paste preparation.

Mixture proportion—The main mixture proportion of UHPC analyzed in this study for investigation is shown in Table 2.

Specimen preparation

Mortar preparation—Fine river sand, cementitious material, and mineral admixture were first added into the dry mixer and mixed for 1 minute. Then, the mixture was mixed with water and HRWRA for 4 minutes. Finally, steel fiber was slowly added into and mixed together for 3 minutes. The prepared mortar was placed in a 40 x 40 x 160 mm mold.

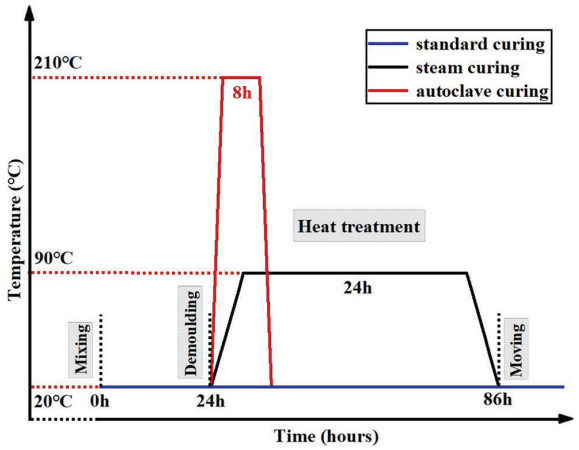

Fig. 2—Different curing regimes of UHPC.

After being vibrated and smoothed to shape, the molds were covered with impermeable film in the standard environment for 24 hours.

Paste preparation—First, cement and mineral admixture were added into a dry mixer and mixed for 1 minute. Then the water and HRWRA were added together and continued to be stirred for more than 4 minutes. Finally, the prepared paste was placed into a ϕ10 x 50 mm plastic pipe. After standard curing for 24 hours, the specimens were detached from the mold.

Curing regimes

Three types of curing regimes, shown in Fig. 2, were used in this study. The curing temperature, curing pressure, and curing time are found in the references.[14,17,19,29,30]

Standard curing—The specimens detached from the mold were cured under the standard environment (20 ± 3°C, relative humidity > 95%) to the corresponding curing age.

Steam curing—The specimens detached from the mold were first moved into a rapid concrete curing box (constant temperature: 90°C, heating rate: 10°C/h) and cured at 90°C for 48 hours. After natural cooling, the specimens were moved into standard curing environment and cured until the test curing age (3, 7, and 28 days).

Autoclave curing—The specimens detached from the mold were first moved into the autoclave (constant temperature: 210°C, pressure: 2 MPa, temperature and pressure reached within 2.5 hours) and cured under 210°C, 2 MPa condition for 8 hours. After natural cooling, the specimens were moved to the standard curing environment and cured to the corresponding test age.

EXPERIMENTAL METHODOLOGY

Mechanical properties

According to GB/T 50081-2019, the mechanical strength of specimens was tested at specific curing ages. There are three samples in each group, and the average value is calculated after testing the compressive strength.

X-ray diffraction analysis

In aspect to the treatment of test samples, the ϕ10 x 50 mm specimens cured to the specific curing age were processed through the following steps: 1) the specimens were cracked to a particle size of approximately 2 to 3 mm granular samples and soaked in anhydrous ethanol solution to terminate hydration; and 2) the no-longer-hydrated granular samples were dried at 40°C under vacuum for 2 hours, then ground and passed through a mesh sieve. The crystal structures and phase composition of specimens obtained through the aforementioned steps were tested by a diffractometer with CuKα1 radiation. The test was carried out using a 2θ angle range of 5 to 70 degrees with a step size of 0.02 degrees. The scanning speed of the test ws 5 deg/min.

Scanning electron microscopy (SEM)

The no-longer-hydrated granular samples, obtained through the steps mentioned previously, were used as test samples. A field-emission environmental scanning electron microscope was used to characterize the microstructure and micromorphology of the specimens. Moreover, an X-ray energy spectrometer (EDS) was also used to analyze the microzone composition of the samples.

Nuclear magnetic resonance (NMR) spectroscopy

The samples used in ^{29}Si NMR and ^{27}Al NMR were the same as those used in XRD analysis. The magic-angle rotation speeds were 8 and 12 kHz. The resonant frequencies of ^{29}Si and ^{27}Al were 79.3 and 104 MHz, the pulse widths were 4.0 and 0.5 μs, and the number of scans were all 12,000. The relative intensity values (I) of characteristic peaks of ^{29}Si NMR and ^{27}Al NMR spectra were calculated through PeakFit software. Meanwhile, the obtained relative intensity values (I) could be further calculated, according to Eq. (1) to (4), to obtain the hydration degree, the MCL of silicate chains in calcium (alumino)silicate hydrate (C-(A)-S-H) gels, and the degree of Al^{3+} substitution for Si^{4+} (Al[4]/Si)[31-33]

$$\alpha_C = 1 - I(Q^0)/I_0(Q^0) \quad (1)$$

$$\alpha_{SF+Q} = 1 - I(Q^3 + Q^4)/I_0(Q^3 + Q^4) \quad (2)$$

$$MCL = 2[I(Q^1) + I(Q^2) + 1.5Q^2(1Al)]/I(Q^1) \quad (3)$$

$$Al[4]/Si = 0.5I(Q^2(1Al))/[I(Q^1) + I(Q^2(0Al)) + I(Q^2(1Al))] \quad (4)$$

where α_C and α_{SF+Q} denote the hydration degree of cement and the hydration degree of silica fume/quartz powder in UHPC, respectively; $I_0(Q^0)$ denotes the relative intensity of the Q^0 integral area in the cement when the cementitious material of UHPC is unhydrated; $I(Q^0)$ denotes the relative intensity of the Q^0 integral area of residual unhydrated cement in the hardened paste; $I_0(Q^4)$ and $I(Q^4)$ denote the relative intensity of the Q^4 integrated area in the unhydrated silica fume/quartz powder and the hardened paste, respectively; and $I(Q^1)$, $I(Q^2)$, and $I(Q^2(1Al))$ denote the relative intensities of the Q^1, Q^2, and $Q^2(1Al)$ integrated areas in the hardened paste, respectively.

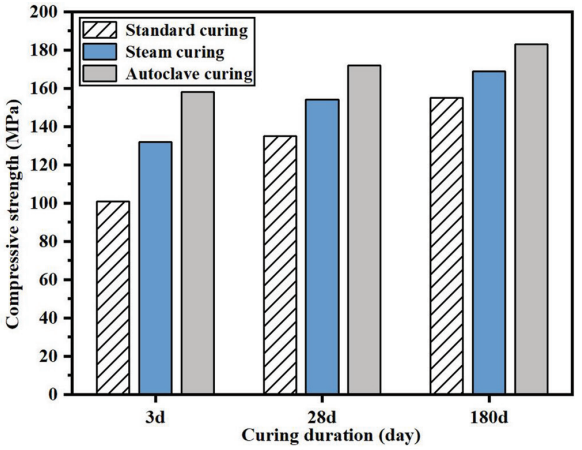

(a) The compressive strength of UHPC

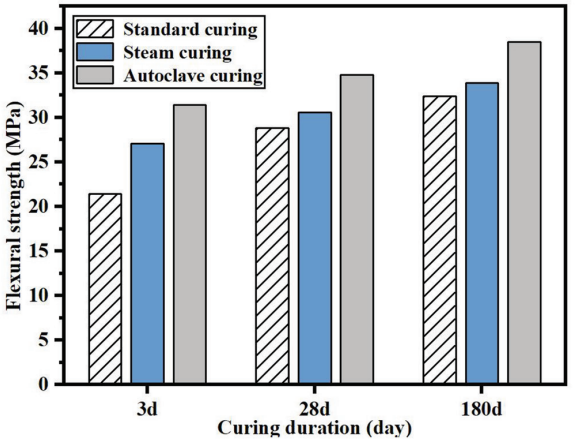

(b) The flexural strength of UHPC

Fig. 3—Mechanical properties of UHPC under different curing regimes.

EXPERIMENTAL RESULTS AND DISCUSSION

Effect of curing regimes on mechanical properties of UHPC

Figure 3 shows the compressive strength and flexural strength of UHPC cured to 3, 28, and 180 days under three different curing regimes (standard curing, steam curing at 90°C, and autoclave curing at 210°C and 2 MPa).

From Fig. 3, it can be seen that the compressive and flexural strength of specimens increased with the increase of curing temperature at the same curing age. Compared with that of specimens with standard curing, the 3-day compressive strength of specimens with steam curing and autoclave curing increased by 30.69% and 56.44%, respectively, and the 3-day flexural strength of specimens with steam curing and autoclave curing increased by 26.64% and 46.73%, respectively. When the curing age reached 180 days, the compressive strength of specimens with steam curing and

autoclave curing increased by 9.03% and 18.06%, respectively, and the flexural strength increased by 4.63% and 18.83%, respectively. This phenomenon could be attributed to the fact that the high temperature and pressure of curing regimes promoted the hydration of cement and pozzolanic reaction of silica fume/quartz powder. The higher hydration degree resulted in more hydration products and a higher crystallization degree, which improved the mechanical performance of UHPC.[12] Moreover, it can also be found that the strength growth rate with the increased curing age for different curing regimes is: standard curing > steam curing > autoclave curing. This may be attributed to the fact that for the standard curing samples, the hydration process of cement and mineral admixtures is a long-term and slow process. Although the amount of early hydration products is relatively small and the porosity is large, the hydration products and the compactness continue to increase with the increase of the age, which made the mechanical properties improve greatly in the later stage. For the steam and autoclave curing specimens, heat treatment increased the hydration degree of cement and silica fume/quartz powder in the early curing age. A large amount of formed hydration products built around the cementitious material, affecting the diffusion process of subsequent hydration and resulting in reduced increase in compressive strength and flexural strength in later stages.[12]

Phase composition

The XRD patterns of specimens under three different curing regimes are shown in Fig. 4. As can be seen from Fig. 4(a), under the standard curing regime, the hydration products of specimens at different curing ages all mainly contained ettringite, $Ca(OH)_2$, and unhydrated C_3S and β-C_2S phases. With the extension of the curing age, the diffraction peak intensity of C_3S and β-C_2S phases gradually decreased and were consumed in the process of hydration. Meanwhile, the $Ca(OH)_2$ content also decreased with the extension of curing age, which could be attributed to the fact that $Ca(OH)_2$ generated by cement hydration was consumed by the pozzolanic reaction of silica fume/quartz powder in the specimen. However, no matter how long the curing age, the diffraction peak intensity of ettringite (AFt) was always in a low state, which is the same as in previous studies.[16,34] This may be due to the fact that the dense structure of UHPC influenced the growth of AFt.

From Fig. 4(b) and (c), it can be seen that the varied patterns of hydration products of UHPC under different curing regimes are similar. Compared with specimens under standard curing regimes, the intensity of diffraction peaks of AFt and $Ca(OH)_2$ decreased significantly with the increase of curing temperature and pressure. When the curing temperature and pressure reached 210°C and 2 MPa, the presence of both AFt and $Ca(OH)_2$ was no longer detected in the XRD pattern. This is because high temperature and high pressure could not only effectively promote the hydration of cement and the pozzolanic reaction in UHPC, but also made AFt decompose and convert to other phases.[35] Moreover, it can be seen that there is another peak of tobermorite (T) in the XRD pattern of the autoclave curing specimens, which does

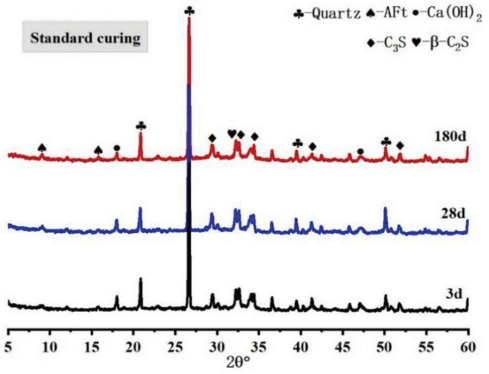

(a) The XRD pattern of specimen with standard curing

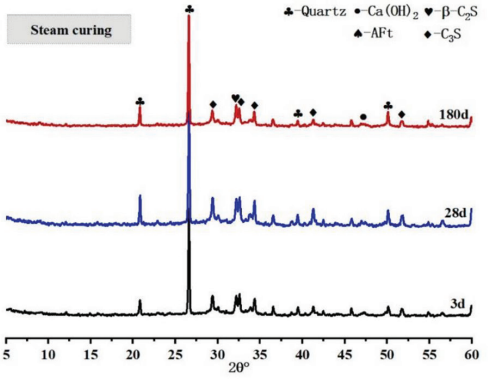

(b) The XRD pattern of specimen with steam curing

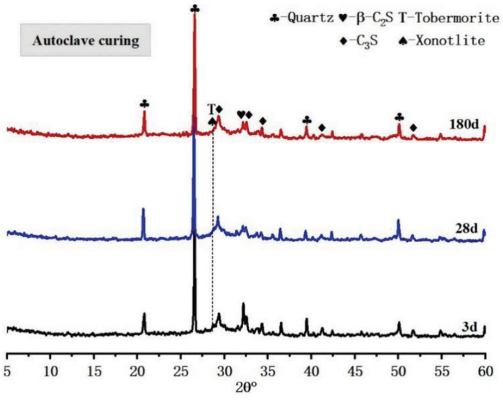

(c) The XRD pattern of specimen with autoclave curing

Fig. 4—XRD patterns of specimens under different curing regimes.

not appear in the XRD pattern of the standard curing specimens and steam curing specimens. As mentioned in peer literature,[14,18] this phenomenon could be attributed to the fact that the high curing temperature and pressure of autoclaved curing involved more Al^{3+}, as well as Si^{4+}, in the silicate chain and improved the polymerization degree of the hydration product (tobermorite). The high packing density and stiffness of tobermorite could also explain the higher compressive strength of autoclaved cured samples to some extent.

Micromorphology

The microstructure of specimens cured under three different curing regimes are shown in Fig. 5. It can be seen from

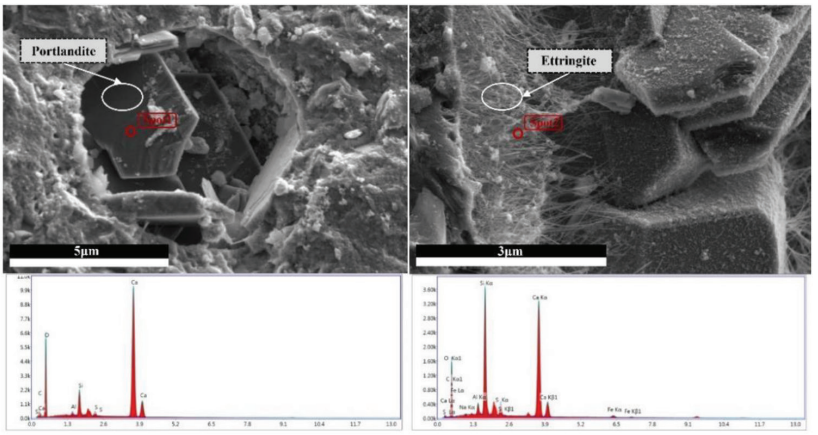

(a) SEM spectra of hydration products in specimen with standard curing

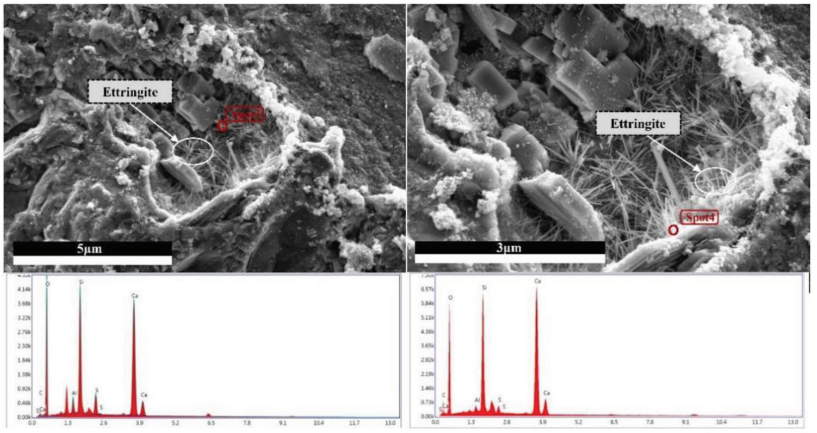

(b) SEM spectra of hydration products in specimen with steam curing

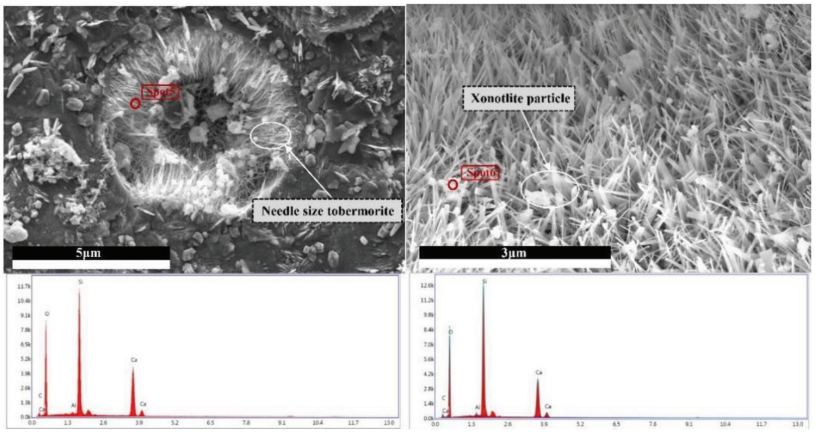

(c) SEM spectra of hydration products in specimen with autoclave curing

Fig. 5—SEM-EDS spot analysis of UHPC under different curing regimes.

Fig. 5(a) that there was a large amount of portlandite as well as needle-like AFt in the sample standard cured for 180 days. When the curing temperature increased to 90°C, the amount of portlandite and AFt gradually decreased. This phenomenon is the same as described in the "Phase composition" section, which confirms that the steam curing regime promoted the hydration reaction in UHPC. When the curing temperature and curing pressure increased further to 210°C and 2 MPa, respectively, the portlandite content is further reduced. Needle-size tobermorite began to appear in the micromorphology of UHPC. Moreover, some xonotlite particles transformed from tobermorite can even be observed in the SEM image. This can verify that high curing temperature increased the crystallization and polymerization of the gel.

From the EDS spectra of specimens under the different curing regimes, it can be found that the Si/Ca ratio of needle hydration products at point 1 and point 3 is approximately 0.70, which is ettringite, and the Si/Ca ratio of needle hydration products increased to 1.81 for the specimen with autoclave curing.[11,36] This phenomenon clarifies that: 1) higher curing temperature enhanced the pozzolanic reaction of silica fume/quartz powder, which provided more Si^{4+} for the

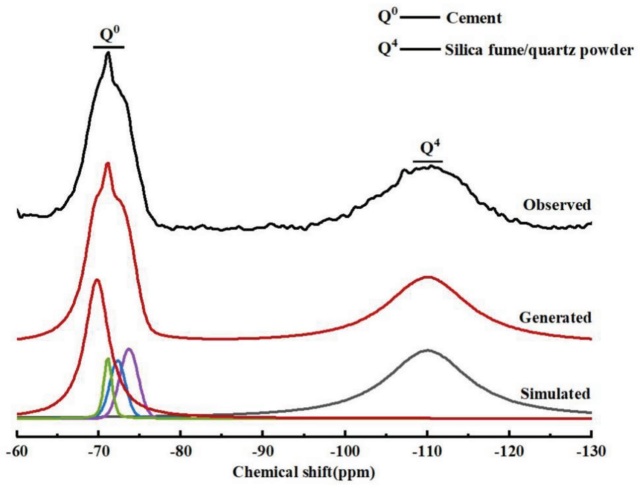

Fig. 6—^{29}Si NMR spectra of cementitious material.

formation of C-S-H gel and increased the Si/Ca ratio as well as the polymerization degree of the gel; and 2) a high Si/Ca ratio is necessary to improve the polymerization degree of hydration products, which could promote Al^{3+} incorporation into C-S-H gel and increase the MCL.[37] Generally, the autoclave curing regime promoted the pozzolanic reaction of silica fume/quartz powder in specimens, which incorporated more Si^{4+} in the gel structure and formed higher-stiffness hydration products (such as tobermorite and xonotlite).[38]

^{29}Si NMR

To characterize the hydration degree of specimens with different curing regimes, ^{29}Si NMR was used in this paper. Meanwhile, to analyze the ^{29}Si NMR spectra more accurately, ^{29}Si NMR was also performed on the raw cementitious material. As shown in Fig. 6 and 7, the ^{29}Si NMR spectra of different specimens are carried on according to the Q_n-Quotation, where Q represents the silicon-oxygen tetrahedron unit and n represents the degree of connectivity. The resonance peak Q^0, located at –71.0 ppm, corresponds to tricalcium silicate and dicalcium silicate in the cement. The amorphous SiO_2 in the silica fume/quartz powder exhibits Q^4 at approximately –110.5 ppm. $Q_0(H)$ represents the hydrated silicon-oxygen tetrahedral monomer, displaying peak at approximately –75.7 ppm. The C-S-H phase presents Q^1, Q^2(1Al), Q^{2B}, and Q^{2P} units from its chain structure at approximately –78.7, –80.1, –82.2, and –84.2 ppm, respectively. Q^1, Q^{2B}, Q^{2P}, and Q^2(1Al) denote the silicate tetrahedra in the C-(A)-S-H gel chain terminals, chain bridging places, and paired sites with an aluminate tetrahedron coordination.[27]

The deconvolution results of specimens with different curing regimes are shown in Table 3. Combined with Fig. 7, it can be seen that under the same curing age, the relative strength value of Q^0 and Q^1 of different curing regimes shows the trend that autoclave curing < steam curing < standard curing. C-S-H gel under standard curing mainly exists as dimer (Q^1),[39,40] as shown in Fig. 8. With the increase of curing temperature and pressure, the ion diffusion rate of cementitious materials during hydration was improved, which promoted the

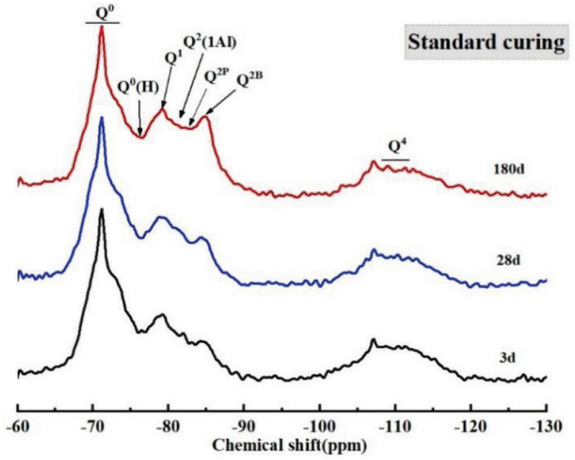

(a) The ^{29}Si NMR spectra of standard curing

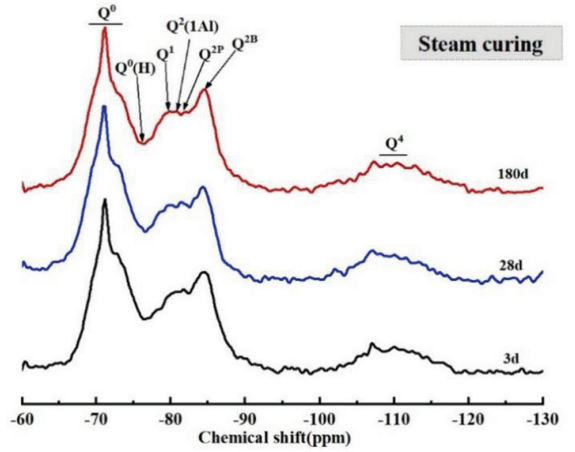

(b) The ^{29}Si NMR spectra of steam curing

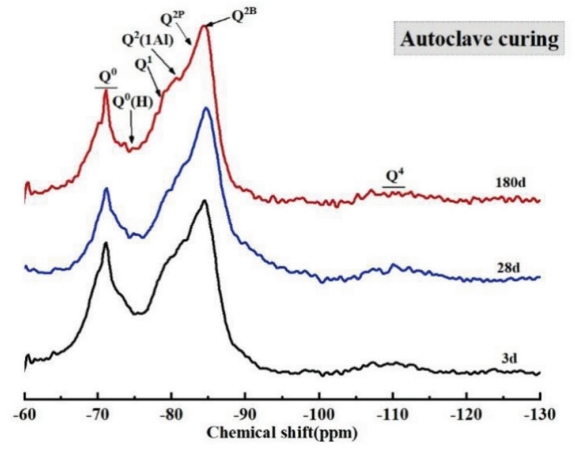

(c) The 29Si NMR spectra of autoclave curing

Fig. 7—^{29}Si NMR spectra of UHPC under different curing regimes.

hydration kinetics of cement and silica fume/quartz powder. Thus, the relative strength value of Q^0 and Q^4 in the specimens decreased and more Al^{3+} and Si^{4+} worked as bridging tetrahedra between silicate units. AlO_4 and SiO_4 bridging tetrahedra increased the MCL and polymerization degree of C-S-H gel,[40] which could be verified by the decreased relative

Table 3—Deconvolution results of ^{29}Si NMR spectra

Curing regimes	Curing age, days	Relative strength value of Q^n, %							α_C, %	α_{SF+Q}, %	MCL	Al[4]/Si
		Q^0	$Q^0(H)$	Q^1	Q^2(1Al)	Q^{2B}	Q^{2P}	Q^4				
Standard curing	3	44.3	1.0	19.6	0	2.5	5.0	36.6	28.5	3.6	2.8	0
	28	33.1	3.3	19.8	1.8	3.1	6.3	32.6	46.6	14.2	3.2	0.03
	180	30.1	5.2	19.4	3.4	3.9	7.8	29.8	51.5	21.6	3.7	0.05
Steam curing	3	36.5	8.7	12.9	11.9	4.1	8.1	27.3	41.1	28.2	6.5	0.16
	28	31.6	6.6	12.2	8.5	5.3	10.6	25.2	49.0	33.7	6.7	0.11
	180	27.9	5.7	11.9	7.3	8.2	16.4	22.6	55	40.5	8.0	0.08
Autoclave curing	3	27.3	1.5	12.7	18.2	9.2	18.4	13.6	57.4	64.2	10.3	0.16
	28	26.4	1.0	12.0	14.2	12.8	25.6	10.7	61.8	71.8	12.0	0.11
	180	20.3	0.8	11.8	13.4	15.1	30.2	8.4	67.2	77.9	13.1	0.10

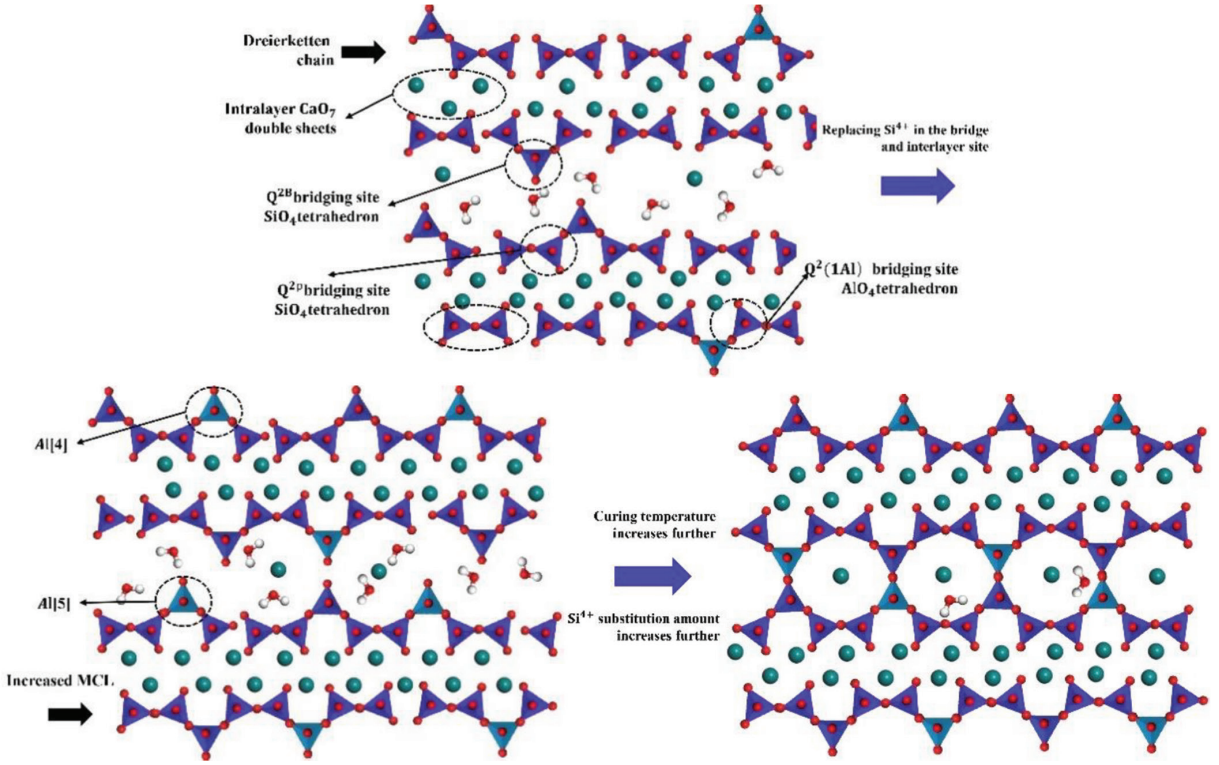

Fig. 8—Variation of silicate chain with increased curing temperature.

strength value of Q^1. Moreover, from Table 3, it can also be seen that the change trend of Q^2(1Al), Q^{2B}, and Q^{2P} units of different curing regimes is contrary to that of Q^0, Q^1, and Q^4, which could be attributed to the fact that Q^2(1Al), Q^{2B}, and Q^{2P} were transformed from Q^0, Q^1, and Q^4. Thus, the higher relative strength value of Q^1, Q^2(1Al), Q^{2B}, and Q^{2P} signify the presence of a higher amount of C-S-H gel and crystal hydration products in the specimens with autoclave curing and steam curing. For further discussion, the hydration degree of cement (α_C), hydration degree of silica fume + quartz powder (α_{SF+Q}), MCL, and ratio of tetracoordinated aluminum to silicon (Al/Si) of the specimens with different curing regimes are calculated and listed in Table 3.

Hydration degree—From Table 3, it can be found that the α_C of the specimens with autoclave curing is 51.0% at 3 days, 55.8% at 28 days, and 62.6% at 180 days, which is much higher than those of the specimens with standard curing and steam curing at the same curing age. Meanwhile, it can be seen that the α_{SF+Q} of specimens with different curing regimes show the same change trend. Thus, it confirmed that the increased curing temperature and the exerted curing pressure promoted the hydration kinetics of cement and silica fume/quartz powder. However, it could also be seen from Table 3 that the α_C and α_{SF+Q} long-term growth rate of the specimen with autoclave curing was slower than those of the other curing regimes. When the curing age of the autoclave curing specimens increased from 3 to 180 days, the growth rates of α_C and α_{SF+Q} were only 9.8% and 13.7%, respectively, which is the same with the change trend of compressive strength. This may be attributed to the fact that the formation of a large amount of hydration products wrapped around the cementitious particles impeded the diffusion of ions and affected the subsequent hydration of the cement. The lower the amount of $Ca(OH)_2$ generated from the hydration of cement, the

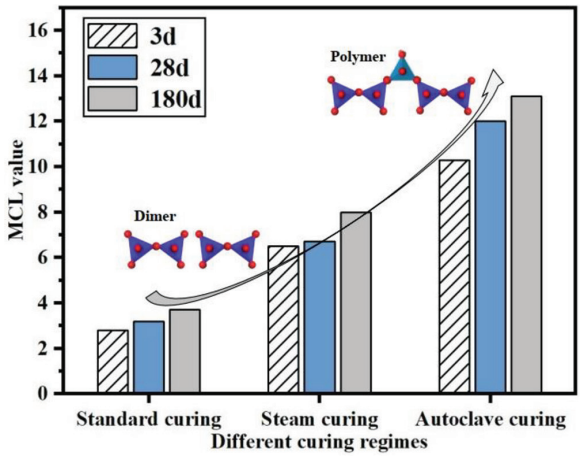

Fig. 9—MCL of specimens with different curing regimes.

lower the hydration degree of silica fume/quartz powder. Thus, the strength growth at later stages was slowed down. Accordingly, it could be concluded that the increased curing temperature and pressure promote the hydration reaction of cement and silica fume/quartz powder at the early stage, but had a negative effect on the long-term hydration process.

MCL—It can be found from Table 3 that the MCL of the specimens with standard curing, steam curing, and autoclave curing at 3 days' curing age are 2.5, 4.1, and 9.2, respectively. As shown in peer literature,[40,41] the MCL of the specimens with standard curing is small, which confirms that the silicate chain in traditional cement-based material is mainly dimer. Meanwhile, according to the linear relationship between MCL and curing temperature, it can also be concluded that a higher curing temperature could promote more Al^{3+} and Si^{4+} working as bridging tetrahedra between silicate units and increase the MCL of the specimens, as depicted in Fig. 9. Moreover, from Table 3, it can also be seen that the MCL of specimens with different curing regimes all increased with curing age. When the curing age reached 180 days, the MCL of specimens with standard curing, steam curing, and autoclave curing are 3.9, 8.2, and 15.1, respectively. This phenomenon confirms that although a longer curing age could increase the hydration and polymerization degree of hydration products, the MCL of the tested specimens do not change greatly, and high-stiffness hydration products (such as tobermorite) in the autoclave curing samples did not appear in the standard curing samples. This confirms the value of heat treatment in UHPC curing.

Al[4]/Si ratio—When the curing age is the same, the relationship of the Al[4]/Si ratio of different specimens is autoclave curing > steam curing > standard curing. Increased curing temperature involved more Al^{3+} in the bridging site of the silicate chain, which contributed to the increased MCL. Meanwhile, considering that the total amount of aluminum ions is constant, this phenomenon could also verify that a higher curing temperature decreased the formation of aluminum-phase hydration products at the early stage. Although the Al[4]/Si ratio of the steam curing specimen at 3 days' curing age is similar to that of the autoclave curing specimen, no tobermorite was detected in the steam curing sample. From the combined MCL calculation data shown in Table 3, it can be inferred that the hydration product with a higher polymerization degree in steam curing samples mainly exists in intermediate products such as C-S-H(I), C-S-H(II), and α-C_2SH.[41,42] Thus, it can be concluded that although the incorporation of Al could extend the MCL of the specimens, its function is limited, and the Si/Ca ratio of gel is a necessary condition for further improving the polymerization degree of hydration products.

Moreover, it can also be found from Table 3 that apart from the specimens with standard curing, the Al[4]/Si ratio of specimens with steam curing and autoclave curing decreased (from 0.16 at 3 days' curing age to 0.08 and 0.10 at 180 days' curing age). This phenomenon could be attributed to the fact that the material containing a large amount of active Al^{3+} (such as C_3A) reacted faster in the early reaction stage and more Al^{3+} was released and absorbed into the gel. This phenomenon made the Al[4]/Si ratio of specimens with steam curing and autoclave curing higher at the early stage. With the extension of the curing age, the unhydrated cement and active SiO_2 in the silica fume/quartz powder continued to hydrate and generate increasing amounts of silica-oxygen tetrahedra, making the Al[4]/Si of the C-S-H gel lower. As a previous study reported,[43] the strength of the Si-O-Si bonds is higher than those of Si-O-Al and Al-O-Al, which accounts for continued growth in long-term strength. Nevertheless, it can be concluded that during the early reaction stage, the C-S-H gel with higher Al[4]/Si had a higher reaction degree and crystallization degree. As the reaction proceeds, more Si^{4+} is involved in the C-S-H gel construction, reducing the Al[4]/Si ratio of C-S-H and improving the long-term stability of the gel.

^{27}Al NMR

The composition of Al-phase products of different specimen are characterized by the ^{27}Al NMR spectrum to explore the effect of different curing regimes on the properties of UHPC. Figure 10 shows the ^{27}Al NMR spectra of specimens with different curing regimes, and the deconvolution results of these specimens are shown in Table 4. The resonance peaks, located at 13.1, 9.8, and 3.9 ppm, are attributed to AFt (Al[6]-E), AFm (Al[6]-M), and TAH (Al[6]-T), respectively. TAH is an amorphous octahedral coordination aluminate phase in the form of $OxAl(OH)_{6-x}^{(3+x)-}$.[32,44] The chemical shift at 35.4 ppm peak is related to Al[5] in the interlayer of C-(A)-S-H gel. The broad resonance centered at approximately 67.2 ppm is attributed to Al[4] in the C-(A)-S-H structure. Moreover, the resonance peak Al[4] in the unhydrated cement is mainly located at approximately –81.0 ppm. Combined with Fig. 10 and Table 4, it can be seen that for the specimens with standard curing and steam curing, Al^{3+} is mainly presented as Al[4] in the C-(A)-S-H gel structure. Meanwhile, for the autoclave curing specimen at 3 days' curing age, Al[4] and Al[5] reached 51.3 and 6.6, respectively. It manifests that Al^{3+} began to be present as Al[5] in the interlayer of C-(A)-S-H gel, which decreased the layer spacing of the gel and balanced the negative charge caused by the replacement of Si^{4+} with Al^{3+}.[32,44,45] Accordingly, the polymerization degree and crystallization degree of C-S-H gel was enhanced, as illustrated in Fig. 8.

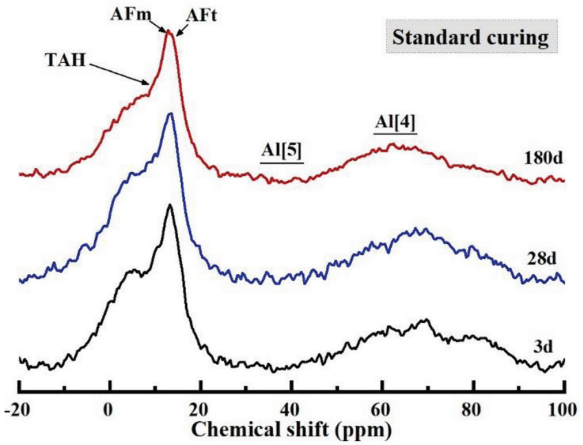

(a) The ^{27}Al NMR spectra of standard curing

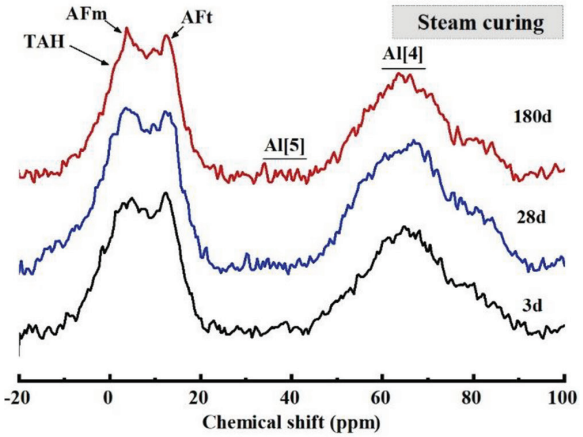

(b) The ^{27}Al NMR spectra of steam curing

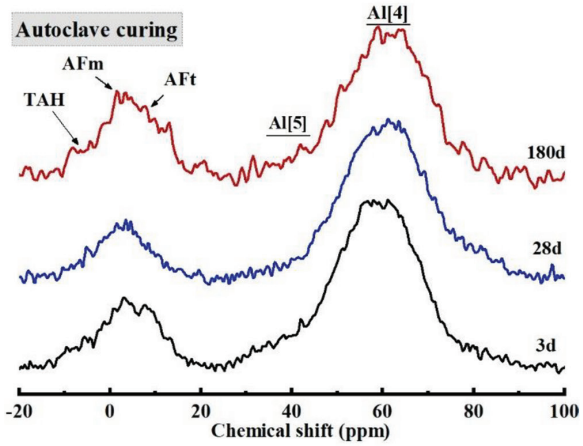

(c) The ^{27}Al NMR spectra of autoclave curing

Fig. 10—^{27}Al NMR spectra of UHPC under different curing regimes.

From Table 4 and Fig. 10, it can also be seen that for the specimens with different curing regimes, the relative content of AFt and AFm increased with the rise of curing age. However, the relative content of TAH shows a different change trend: it decreased with the increase of curing age. It could be concluded that with the extension of curing age,

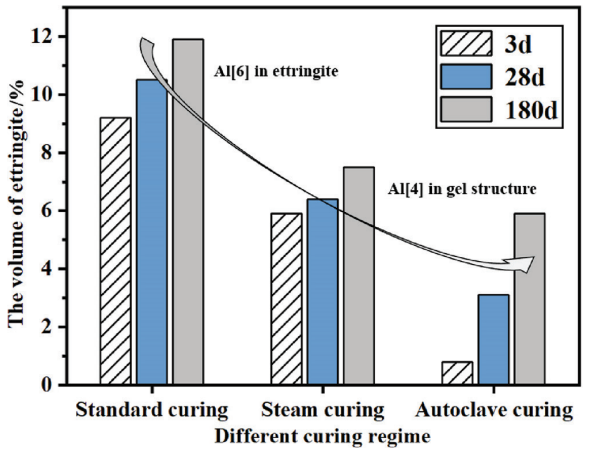

Fig. 11—Volume of ettringite change with curing regime.

TAH gradually converted to AFt and AFm. Moreover, as shown in Fig. 11, it can be seen that the relative content of AFt and AFm at the same curing age decreased with the increase of curing temperature. Combined with the increase of Al[4] and Al[5], this phenomenon could be attributed to the fact that: 1) higher curing temperature affected the formation of AFt and AFm; and 2) the higher polymerization and crystallization degree of cementitious material absorbed large amount of Ca^{2+} and Al^{3+} into the gel structure (Al[4] in aluminum hydration product transformed to Al[4] in gel structure). Compared with specimens under the standard curing regime, on the basis of no other aluminum source material, it can be concluded that Al, Ca, and other ions decomposed from AFt are beneficial to the formation of hydation products with a higher polymerization degree (such as tobermorite or xonotilite).

CONCLUSIONS

A comprehensive investigation was carried out on the composition of hydration products, calcium-silicate-hydrate (C-S-H) gel microstructure, and migration and evolution of aluminum-phase hydration products of cement/silica fume-quartz powder system ultra-high-performance concrete (UHPC) under three curing regimes (standard curing at 20°C, steam curing at 90°C, and pressure steam curing at 210°C and 2 MPa). The following conclusions could be drawn:

1. Heat treatment promotes the hydration of cement and pozzolanic reaction of mineral admixtures, which results in the improvement of compressive strength and flexural strength. The early increase in compressive and flexural strength of the specimen with heat treatment was large, and the 3-day compressive and flexural strengths of the autoclave curing samples were 56.44 and 46.73% higher than those of standard curing specimens. However, the large amount of formed hydration products affected the further hydration of the cementitious material, which slowed down the growth of long-term strength.

2. Compared with the hydration products with a low Si/Ca ratio of standard cured products, the Si/Ca ratio of hydration specimens and the specimens with autoclave curing was increased to 1.81. With the increase of curing temperature

Table 4—Deconvolution results of ^{29}Si NMR spectra

Curing regimes	Curing age, days	Al^{3+} relative strength, %					
		Al[6]-T	Al[6]-M	Al[6]-E	Al[5]	Al[4]	Al[4] in unhydrated cement
Standard curing	3	39.3	3.9	9.2	0	22.7	25.1
	28	35.1	5.2	10.5	0	28.5	22.2
	180	32.2	7.1	11.9	0	34	14.7
Steam curing	3	42.4	0.8	5.9	0	25.5	17.4
	28	39.3	1	6.4	0	29.4	16.4
	180	36.9	1.5	7.5	0	31.3	15.8
Autoclave curing	3	35.7	0.8	0.8	6.6	51.3	4.1
	28	27.3	1.2	3.1	7.1	58.6	2.7
	180	19.7	1.7	5.9	7.6	66.1	1.1

and curing pressure, the polymerization degree of the hydration products of the samples continued to increase, and more silicon and aluminum ions participated in construction of the gel structure.

3. The increased curing temperature and pressure resulted in the higher degree of hydration. More Si^{4+} entered as Q^1, Q^2(1Al), Q^{2B}, and Q^{2P} into the C-S-H gel, which is beneficial to the formation of hydration products. Moreover, the mean chain length (MCL) and Al[4]/Si of the C-S-H gel also increased with the increased curing temperature, implying that the increased temperature allows more Al^{3+} to replace Si^{4+} into the C-S-H gel structure, resulting in growing chain length and increased polymerization of the early C-S-H gel. However, the polymerization effect of Al ions is limited, so the provision of the silicon source to improve the Si/Ca ratio of the system is also important.

4. With the increase of curing temperature, Al^{3+}, originally formed as Al[6] in UHPC, transformed to Al[4] and Al[5] in the gel structure. With the extension of curing age, more and more Si^{4+} decomposed from raw material and became involved in the formation of calcium-(alumino)silicate-hydrate (C-(A)-S-H), which resulted in the decrease of Al[4]/Si of UHPC. The ever-decreasing Al[4]/Si (the strength of Si-O-Si is higher that Al-O-Al or Al-O-Si) explains the long-term increase in mechanical strength of UHPC.

AUTHOR BIOS

Hao Qian *is a Researcher at Anhui Jianzhu University, Hefei, Anhui, China. He received his master's degree from Nanjing Tech University, Nanjing, Jiangsu, China, in 2022. His research interests include three-dimensional (3-D) construction printing materials and ultra-high-performance concrete.*

Gaozhan Zhang *is a Professor at Anhui Jianzhu University. He received his PhD in materials science from Wuhan University of Technology, Wuhan, Hubei, China, in 2017. His research interests include basic theoretical research and engineering application research of advanced cementitious composites.*

Jun Yang *is a Lecturer at Anhui Jianzhu University. He received his PhD in materials science from Wuhan University of Technology in 2019. His research interests include high-performance cement-based materials and radiation-resistant concrete.*

Qingjun Ding *is a Professor at Wuhan University of Technology, where he received his PhD in materials science in 2009, and is a member of the expert group of the Building Materials Science and Technology Engineering Consulting Department of Hubei Science and Technology Consulting Service Center.*

Chundong Geng *is a Researcher at Wuhan University of Technology. His research interests include the planning, consulting, survey, and design of water conservancy and hydropower projects.*

Sudong Hua *is a Professor at Nanjing Tech University. His research interests include the recycling of industrial solid waste and study of 3-D construction printing materials.*

ACKNOWLEDGMENTS

Financial support from the National Natural Science Foundation of China under Grant U21A20149; the Ecological Environment Scientific Research Project of Anhui Province (Grant No. 2023hb0014); the Research Reserve of Anhui Jianzhu University under Grant 2022XMK01; and the Excellent Scientific Research and Innovation Team in Colleges and Universities of Anhui Province under Grant 2022AH010017 is gratefully acknowledged.

REFERENCES

1. Jung, M.; Park, J.-S.; Hong, S.-G.; and Moon, J., "Micro- and Meso-Structural Changes on Electrically Cured Ultra-High-Performance Fiber-Reinforced Concrete with Dispersed Carbon Nanotubes," *Cement and Concrete Research*, V. 137, 2020, p. 106214. doi: 10.1016/j.cemconres.2020.106214

2. Shen, P.; Lu, J.-X.; Lu, L.; He, Y.; Wang, F.; and Hu, S., "An Alternative Method for Performance Improvement of Ultra-High-Performance Concrete by Internal Curing: Role of Physicochemical Properties of Saturated Lightweight Fine Aggregate," *Construction and Building Materials*, V. 312, 2021, p. 125373. doi: 10.1016/j.conbuildmat.2021.125373

3. Hannawi, K.; Bian, H.; Prince-Agbodjan, W.; and Raghavan, B., "Effect of Different Types of Fibers on the Microstructure and the Mechanical Behavior of Ultra-High-Performance Fiber-Reinforced Concretes," *Composites Part B: Engineering*, V. 86, 2016, pp. 214-220. doi: 10.1016/j.compositesb.2015.09.059

4. Yoo, D.-Y., and Yoon, Y.-S., "A Review on Structural Behavior, Design, and Application of Ultra-High-Performance Fiber-Reinforced Concrete," *International Journal of Concrete Structures and Materials*, V. 10, No. 2, 2016, pp. 125-142. doi: 10.1007/s40069-016-0143-x

5. Yazıcı, H.; Yardımcı, M. Y.; Aydın, S.; and Karabulut, A. Ş., "Mechanical Properties of Reactive Powder Concrete Containing Mineral Admixtures under Different Curing Regimes," *Construction and Building Materials*, V. 23, No. 3, 2009, pp. 1223-1231. doi: 10.1016/j.conbuildmat.2008.08.003

6. Matte, V., and Moranville, M., "Durability of Reactive Powder Composites: Influence of Silica Fume on the Leaching Properties of Very Low Water/Binder Pastes," *Cement and Concrete Composites*, V. 21, No. 1, 1999, pp. 1-9. doi: 10.1016/S0958-9465(98)00025-0

7. Yu, R.; Spiesz, P.; and Brouwers, H. J. H., "Mix Design and Properties Assessment of Ultra-High Performance Fibre Reinforced Concrete (UHPFRC)," *Cement and Concrete Research*, V. 56, 2014, pp. 29-39. doi: 10.1016/j.cemconres.2013.11.002

8. Heinz, D.; Urbonas, L.; and Gerlicher, T., "Effect of Heat Treatment Method on the Properties of UHPC," *3rd International Symposium on UHPC and Nanotechnology for High Performance Construction Materials*, Kassel University, Kassel, Germany, 2012, pp. 283-290.

9. Li, W.; Huang, Z.; Hu, G.; Duan, W. H.; and Shah, S. P., "Early-Age Shrinkage Development of Ultra-High-Performance Concrete under Heat Curing Treatment," *Construction and Building Materials*, V. 131, 2017, pp. 767-774. doi: 10.1016/j.conbuildmat.2016.11.024

10. Wille, K.; Naaman, A. E.; El-Tawil, S.; and Parra-Montesinos, G. J., "Ultra-High-Performance Concrete and Fiber Reinforced Concrete: Achieving Strength and Ductility without Heat Curing," *Materials and Structures*, V. 45, No. 3, 2012, pp. 309-324. doi: 10.1617/s11527-011-9767-0

11. Hiremath, P. N., and Yaragal, S. C., "Effect of Different Curing Regimes and Durations on Early Strength Development of Reactive Powder Concrete," *Construction and Building Materials*, V. 154, 2017, pp. 72-87. doi: 10.1016/j.conbuildmat.2017.07.181

12. Prem, P. R.; Bharatkumar, B. H.; and Iyer, N. R., "Influence of Curing Regimes on Compressive Strength of Ultra-High-Performance Concrete," *Sādhanā*, V. 38, No. 6, 2013, pp. 1421-1431. doi: 10.1007/s12046-013-0159-8

13. Yazıcı, H., "The Effect of Curing Conditions on Compressive Strength of Ultra-High Strength Concrete with High Volume Mineral Admixtures," *Building and Environment*, V. 42, No. 5, 2007, pp. 2083-2089. doi: 10.1016/j.buildenv.2006.03.013

14. Shen, P.; Lu, L.; He, Y.; Wang, F.; and Hu, S., "The Effect of Curing Regimes on the Mechanical Properties, Nano-Mechanical Properties and Microstructure of Ultra-High-Performance Concrete," *Cement and Concrete Research*, V. 118, 2019, pp. 1-13. doi: 10.1016/j.cemconres.2019.01.004

15. Courtial, M.; de Noirfontaine, M.-N.; Dunstetter, F.; Signes-Frehel, M.; Mounanga, P.; Cherkaoui, K.; and Khelidj, A., "Effect of Polycarboxylate and Crushed Quartz in UHPC: Microstructural Investigation," *Construction and Building Materials*, V. 44, 2013, pp. 699-705. doi: 10.1016/j.conbuildmat.2013.03.077

16. Wang, D.; Shi, C.; Wu, Z.; Xiao, J.; Huang, Z.; and Fang, Z., "A Review on Ultra-High-Performance Concrete: Part II. Hydration, Microstructure and Properties," *Construction and Building Materials*, V. 96, 2015, pp. 368-377. doi: 10.1016/j.conbuildmat.2015.08.095

17. Hamada, H.; Alattar, A.; Tayeh, B.; Yahaya, F.; and Almeshal, I., "Influence of Different Curing Methods on the Compressive Strength of Ultra-High-Performance Concrete: A Comprehensive Review," *Case Studies in Construction Materials*, V. 17, 2022, p. e01390. doi: 10.1016/j.cscm.2022.e01390

18. Helmi, M.; Hall, M. R.; Stevens, L. A.; and Rigby, S. P., "Effects of High Pressure/Temperature Curing on Reactive Powder Concrete Microstructure Formation," *Construction and Building Materials*, V. 105, 2016, pp. 554-562. doi: 10.1016/j.conbuildmat.2015.12.147

19. Yazıcı, H.; Deniz, E.; and Baradan, B., "The Effect of Autoclave Pressure, Temperature and Duration Time on Mechanical Properties of Reactive Powder Concrete," *Construction and Building Materials*, V. 42, 2013, pp. 53-63. doi: 10.1016/j.conbuildmat.2013.01.003

20. Yang, K. H.; Moon, G. D.; and Jeon, Y. S., "Implementing Ternary Supplementary Cementing Binder for Reduction of the Heat of Hydration of Concrete," *Journal of Cleaner Production*, V. 112, 2016, pp. 845-852. doi: 10.1016/j.jclepro.2015.06.022

21. Ahmed, S.; Al-Dawood, Z.; Abed, F.; Mannan, M. A.; and Al-Samarai, M., "Impact of Using Different Materials, Curing Regimes, and Mixing Procedures on Compressive Strength of Reactive Powder Concrete-A Review," *Journal of Building Engineering*, V. 44, 2021, p. 103238. doi: 10.1016/j.jobe.2021.103238

22. Zhu, Y.; Zhang, Y.; Hussein, H. H.; Liu, J.; and Chen, G., "Experimental Study and Theoretical Prediction on Shrinkage-Induced Restrained Stresses in UHPC-RC Composites under Normal Curing and Steam Curing," *Cement and Concrete Composites*, V. 110, 2020, p. 103602. doi: 10.1016/j.cemconcomp.2020.103602

23. Li, W.; Huang, Z.; Hu, G.; Duan, W. H.; and Shah, S. P., "Early-Age Shrinkage Development of Ultra-High-Performance Concrete under Heat Curing Treatment," *Construction and Building Materials*, V. 131, 2017, pp. 767-774. doi: 10.1016/j.conbuildmat.2016.11.024

24. Manzano, H.; Moeini, S.; Marinelli, F.; Van Duin, A. C. T.; Ulm, F.-J.; and Pellenq, R. J.-M., "Confined Water Dissociation in Microporous Defective Silicates: Mechanism, Dipole Distribution, and Impact on Substrate Properties," *Journal of the American Chemical Society*, V. 134, No. 4, 2012, pp. 2208-2215. doi: 10.1021/ja209152n

25. Cong, X., and Kirkpatrick, R. J., "^{29}Si MAS NMR Study of the Structure of Calcium Silicate Hydrate," *Advanced Cement Based Materials*, V. 3, No. 3-4, 1996, pp. 144-156. doi: 10.1016/S1065-7355(96)90046-2

26. Zhang, G.; Li, Y.; Yang, J.; Ding, Q.; and Sun, D., "Insight into the Strengthening Mechanism of the Al-Induced Cross-Linked Calcium Aluminosilicate Hydrate Gel: A Molecular Dynamics Study," *Frontiers in Materials*, V. 7, 2021, p. 611568. doi: 10.3389/fmats.2020.611568

27. Zou, J.; Guo, C.; Jiang, Y.; Wei, C.; and Li, F., "Structure, Morphology and Mechanism Research on Synthesizing Xonotlite Fiber from Acid-Extracting Residues of Coal Fly Ash and Carbide Slag," *Materials Chemistry and Physics*, V. 172, 2016, pp. 121-128. doi: 10.1016/j.matchemphys.2016.01.050

28. Ipek, M.; Yilmaz, K.; Sümer, M.; and Saribiyik, M., "Effect of Presetting Pressure Applied to Mechanical Behaviors of Reactive Powder Concrete During Setting Phase," *Construction and Building Materials*, V. 25, No. 1, 2011, pp. 61-68. doi: 10.1016/j.conbuildmat.2010.06.056

29. Abdulkareem, O. M.; Ben Fraj, A.; Bouasker, M.; and Khelidj, A., "Effect of Chemical and Thermal Activation on the Microstructural and Mechanical Properties of More Sustainable UHPC," *Construction and Building Materials*, V. 169, 2018, pp. 567-577. doi: 10.1016/j.conbuildmat.2018.02.214

30. Wu, Z.; Shi, C.; and He, W., "Comparative Study on Flexural Properties of Ultra-High-Performance Concrete with Supplementary Cementitious Materials under Different Curing Regimes," *Construction and Building Materials*, V. 136, 2017, pp. 307-313. doi: 10.1016/j.conbuildmat.2017.01.052

31. Zhang, G.; Yang, Q.; Hou, D.; Zhou, P.; and Ding, Q., "Unraveling the Microstructural Properties of Cement-Slag Composite Pastes Incorporated with Smart Polymer-Based Corrosion Inhibitors: From Experiment to Molecular Dynamics," *Cement and Concrete Composites*, V. 125, 2022, p. 104298. doi: 10.1016/j.cemconcomp.2021.104298

32. Zhang, G.; Wu, C.; Hou, D.; Yang, J.; Sun, D.; and Zhang, X., "Effect of Environmental pH Values on Phase Composition and Microstructure of Portland Cement Paste under Sulfate Attack," *Composites Part B: Engineering*, V. 216, 2021, p. 108862. doi: 10.1016/j.compositesb.2021.108862

33. Girão, A. V.; Richardson, I. G.; Taylor, R.; and Brydson, R. M. D., "Composition, Morphology and Nano-Structure of C–S–H in 70% White Portland Cement–30% Fly Ash Blends Hydrated at 55°C," *Cement and Concrete Research*, V. 40, No. 9, 2010, pp. 1350-1359. doi: 10.1016/j.cemconres.2010.03.012

34. Chong, W.; Yang, C.; Fang, L.; Wan, C.; and Pu, X., "Preparation of Ultra-High-Performance Concrete with Common Technology and Materials," *Cement and Concrete Research*, V. 26, No. 4, 2004, pp. 538-544.

35. Kim, S.; Lee, N.; Lee, H. K.; and Park, S., "Experimental and Theoretical Studies of Hydration of Ultra-High-Performance Concrete Cured under Various Curing Conditions," *Construction and Building Materials*, V. 278, No. 7, 2021, p. 122352. doi: 10.1016/j.conbuildmat.2021.122352

36. Chen, T.; Gao, X.; and Ren, M., "Effects of Autoclave Curing and Fly Ash on Mechanical Properties of Ultra-High-Performance Concrete," *Construction and Building Materials*, V. 158, 2018, pp. 864-872. doi: 10.1016/j.conbuildmat.2017.10.074

37. Kapeluszna, E.; Kotwica, Ł.; Różycka, A.; and Gołek, Ł., "Incorporation of Al in C-A-S-H Gels with Various Ca/Si and Al/Si Ratio: Microstructural and Structural Characteristics with DTA/TG, XRD, FTIR and TEM Analysis," *Construction and Building Materials*, V. 155, 2017, pp. 643-653. doi: 10.1016/j.conbuildmat.2017.08.091

38. Hesse, C.; Goetz-Neunhoeffer, F.; and Neubauer, J., "A New Approach in Quantitative In-Situ XRD of Cement Pastes: Correlation of Heat Flow Curves with Early Hydration Reactions," *Cement and Concrete Research*, V. 41, No. 1, 2011, pp. 123-128. doi: 10.1016/j.cemconres.2010.09.014

39. Battocchio, F., and Paulo, J. M., "Rietveld Refinement of the Structures of 1.0 CSH and 1.5 C-S-H," *Cement and Concrete Research*, V. 42, No. 11, 2012, pp. 1534-1548. doi: 10.1016/j.cemconres.2012.07.005

40. Dong, Y.; Feng, C.; Zhao, Q.; and Liang, X., "Study on the Structure of C-S-H Gels of Slag–Cement Hardened Paste by ^{29}Si, ^{27}Al MAS NMR," *Applied Magnetic Resonance*, V. 50, No. 12, 2019, pp. 1345-1357. doi: 10.1007/s00723-019-01152-6

41. Oh, J. E.; Clark, S. M.; and Monteiro, P. J. M., "Does the Al Substitution in C–S–H (I) Change its Mechanical Property?" *Cement and Concrete Research*, V. 41, No. 1, 2011, pp. 102-106. doi: 10.1016/j.cemconres.2010.09.010

42. Dharmawardhana, C. C.; Misra, A.; and Ching, W. Y., "Theoretical Investigation of C-(A)-S-H(I) Cement Hydrates," *Construction and Building Materials*, V. 184, 2018, pp. 536-548. doi: 10.1016/j.conbuildmat.2018.07.004

43. Duxson, P.; Provis, J. L.; Lukey, G. C.; Mallicoat, S. W.; Kriven, W. M.; and van Deventer, J. S. J., "Understanding the Relationship between Geopolymer Composition, Micro-Structure and Mechanical Properties," *Colloids and Surfaces A: Physicochemical and Engineering Aspects*, V. 269, No. 1-3, 2005, pp. 47-58. doi: 10.1016/j.colsurfa.2005.06.060

44. Andersen, M. D.; Jakobsen, H. J.; and Skibsted, J., "A New Aluminum Hydrate Species in Hydrated Portland Cements Characterized by ^{27}Al and ^{29}Si MAS NMR Spectroscopy," *Cement and Concrete Research*, V. 36, No. 1, 2006, pp. 3-17. doi: 10.1016/j.cemconres.2005.04.010

45. Pardal, X.; Pochard, I.; and Nonat, A., "Experimental Study of Si–Al Substitution in Calcium-Silicate-Hydrate (C-S-H) Prepared under Equilibrium Conditions," *Cement and Concrete Research*, V. 39, No. 8, 2009, pp. 637-643. doi: 10.1016/j.cemconres.2009.05.001